REPORT DOCUMENTATION PAGE

Form Approved OMB NO. 0704-0188

1. REPORT DATE (DD-MM-YYYY)	2. REPORT TYPE	3. DATES COVERED (From - To)
10-07-2014	Final Report	11-Apr-2011 - 10-Apr-2014

4. TITLE AND SUBTITLE
Final Project Report - April 11, 2011 to April 10, 2014 for

W911NF-11-1-0129

5a. CONTRACT NUMBER
W911NF-11-1-0129

5b. GRANT NUMBER

5c. PROGRAM ELEMENT NUMBER
206022

6. AUTHORS
Ricardo von Borries

5d. PROJECT NUMBER

5e. TASK NUMBER

5f. WORK UNIT NUMBER

7. PERFORMING ORGANIZATION NAMES AND ADDRESSES
University of Texas at El Paso
500 West University Avenue

El Paso, TX 79968 -0587

8. PERFORMING ORGANIZATION REPORT NUMBER

9. SPONSORING/MONITORING AGENCY NAME(S) AND ADDRESS (ES)
U.S. Army Research Office
P.O. Box 12211
Research Triangle Park, NC 27709-2211

10. SPONSOR/MONITOR'S ACRONYM(S)
ARO

11. SPONSOR/MONITOR'S REPORT NUMBER(S)
59050-CS-REP.7

12. DISTRIBUTION AVAILIBILITY STATEMENT
Approved for Public Release; Distribution Unlimited

13. SUPPLEMENTARY NOTES
The views, opinions and/or findings contained in this report are those of the author(s) and should not contrued as an official Department of the Army position, policy or decision, unless so designated by other documentation.

14. ABSTRACT
In this final report, we indicate the main activities in the period from April 11, 2011, to April 10, 2014. First, we relate the main research objectives of our project to the corresponding activities implemented in support of those objectives, including published papers. Then, we indicate the educational activities implemented in support of the research. This project enabled our research group to attract, engage and retain graduate and undergraduate research assistants into learning advanced science and engineering concepts on compressive sensing, ground penetrating radar, microwave tomography, microwave laboratory instrumentation and distributed computer simulations

15. SUBJECT TERMS
Microwave tomography, compressed sensing, prior information, scanner, radon transform.

16. SECURITY CLASSIFICATION OF:			17. LIMITATION OF ABSTRACT	15. NUMBER OF PAGES	19a. NAME OF RESPONSIBLE PERSON
a. REPORT	b. ABSTRACT	c. THIS PAGE			Ricardo von Borries
UU	UU	UU	UU		19b. TELEPHONE NUMBER 915-747-7959

Report Title

Final Project Report - April 11, 2011 to April 10, 2014

ABSTRACT

In this final report, we indicate the main activities in the period from April 11, 2011, to April 10, 2014. First, we relate the main research objectives of our project to the corresponding activities implemented in support of those objectives, including published papers. Then, we indicate the educational activities implemented in support of the research. This project enabled our research group to attract, engage and retain graduate and undergraduate research assistants into learning advanced science and engineering concepts on compressive sensing, ground penetrating radar, microwave tomography, microwave laboratory instrumentation and distributed computer simulations.

Enter List of papers submitted or published that acknowledge ARO support from the start of the project to the date of this printing. List the papers, including journal references, in the following categories:

(a) Papers published in peer-reviewed journals (N/A for none)

Received Paper

TOTAL:

Number of Papers published in peer-reviewed journals:

(b) Papers published in non-peer-reviewed journals (N/A for none)

Received Paper

TOTAL:

Number of Papers published in non peer-reviewed journals:

(c) Presentations

Number of Presentations: 0.00

Non Peer-Reviewed Conference Proceeding publications (other than abstracts):

Received		Paper
06/01/2013	4.00	M. J. Salvador, V. Jimenez, R. G. Lopez, R. von Borries. Platform for Research and Education on Ground Penetrating Radar, SPIE Defense, Security, and Sensing. 29-APR-13, . : ,
TOTAL:	**1**	

Number of Non Peer-Reviewed Conference Proceeding publications (other than abstracts):

Peer-Reviewed Conference Proceeding publications (other than abstracts):

Received		Paper
09/05/2012	2.00	R. von Borries, B. Verdin. Lidar Range Pro♀le Reconstruction byUsing Chaotic Signals and Compressive Sensing, SPIE Optical Engineering + Applications. 15-AUG-12, . : ,
TOTAL:	**1**	

Number of Peer-Reviewed Conference Proceeding publications (other than abstracts):

(d) Manuscripts

Received		Paper
06/01/2013	3.00	C. J. Miosso, R. von Borries, J. H. Pierluissi. Compressive Sensing with Prior Information $-$ Requirements and Probabilities of Reconstruction in ℓ_1-Minimization, IEEE Tran. on Signal Processing (07 2011)
09/05/2012	1.00	C. J. Miosso, R. von Borries, J.H. Pierluissi. Compressive Sensing with Prior Information - Requirements and Probabilities of Reconstruction in L1-Minimization, ( )
TOTAL:	**2**	

Number of Manuscripts:

Books

Received Book

TOTAL:

Received Book Chapter

TOTAL:

Patents Submitted

Patents Awarded

Awards

Graduate Students

NAME	PERCENT_SUPPORTED	Discipline
Rafael Lopez	0.16	
Guillermo Gonzalez	0.00	
Virginia Jimenez	0.17	
FTE Equivalent:	**0.33**	
Total Number:	**3**	

Names of Post Doctorates

NAME	PERCENT_SUPPORTED
Berenice Verdin	0.00
FTE Equivalent:	**0.00**
Total Number:	**1**

Names of Faculty Supported

NAME	PERCENT_SUPPORTED	National Academy Member
Benjamin Flores	0.00	No
Joseph Pierluissi	0.05	
Ricardo von Borries	0.15	
FTE Equivalent:	**0.20**	
Total Number:	**3**	

Names of Under Graduate students supported

NAME	PERCENT_SUPPORTED	Discipline
Virginia Jimenez	0.83	Computer and Computational Science and Electrical E
Michelle Salvador	0.33	Computer and Computational Science and Electrical E
Alonso Orea	0.33	Computer and Computational Science and Electrical E
Mario Rojas	0.33	Computer and Computational Science and Electrical E
Ricardo Barreto	0.33	Computer and Computational Science and Electrical E
Cesar Soto	0.16	Computer and Computational Science and Electrical E
FTE Equivalent:	**2.31**	
Total Number:	**6**	

Student Metrics

This section only applies to graduating undergraduates supported by this agreement in this reporting period

The number of undergraduates funded by this agreement who graduated during this period: .....

The number of undergraduates funded by this agreement who graduated during this period with a degree in science, mathematics, engineering, or technology fields:.....

The number of undergraduates funded by your agreement who graduated during this period and will continue to pursue a graduate or Ph.D. degree in science, mathematics, engineering, or technology fields:.....

Number of graduating undergraduates who achieved a 3.5 GPA to 4.0 (4.0 max scale):.....

Number of graduating undergraduates funded by a DoD funded Center of Excellence grant for Education, Research and Engineering:.....

The number of undergraduates funded by your agreement who graduated during this period and intend to work for the Department of Defense .....

The number of undergraduates funded by your agreement who graduated during this period and will receive scholarships or fellowships for further studies in science, mathematics, engineering or technology fields: .....

Names of Personnel receiving masters degrees

NAME
Total Number:

Names of personnel receiving PHDs

NAME
Total Number:

Names of other research staff

NAME	PERCENT_SUPPORTED
FTE Equivalent:	
Total Number:	

Sub Contractors (DD882)

Inventions (DD882)

Scientific Progress

(In Attachment)

Technology Transfer

Final Project Report – April 11, 2011 to April 10, 2014

Proposal Number: **W911NF-11-1-0129, DoD, HBCU/MSI**
Research Category: **Basic Scientific Research**
Topical Area: **Sensors and Detectors**
Proposal Title: **Detection and Imaging of Improvised Explosive Devices**
Institution: **University of Texas at El Paso**
Department: **Electrical and Computer Engineering**
Address: **500 W. University Av., Engineering Room A325, El Paso, TX, 79968**
Principal Investigator: **Ricardo von Borries**

Summary

In this final report, we indicate the main activities in the period from April 11, 2011, to April 10, 2014. First, we relate the main research objectives of our project to the corresponding activities implemented in support of those objectives, including published papers. Then, we indicate the educational activities implemented in support of the research. This project enabled our research group to attract, engage and retain graduate and undergraduate research assistants into learning advanced science and engineering concepts on compressive sensing, ground penetrating radar, microwave tomography, microwave laboratory instrumentation and distributed computer simulations.

Contents

1 Research Objectives

This section indicates the main research objectives stated in our project and their corresponding research activities implemented in the period of April 2011 to April 2014.

1.1 Objective 1

To determine whether compressive sensing can provide image reconstruction with improved resolution.

The PhD graduate student Lopez, Master graduate student Jimenez and von Borries developed a set of Matlab functions to: (1) generate the circular projections (central slice theorem) on the Fourier plane (implemented two options to simulate the tomography data projections: modeling the direct problem in tomographic imaging with diffraction or generating projections using sampling on circular trajectories in the Fourier plane); (2) select a subset of the sampling points on the circular trajectories in the Fourier plane; (3) generate the filter bank decomposition of those selected Fourier samples into sparse components (two-dimensional high-pass components) and non-sparse component (two-dimensional low-pass component); (4) reconstruct the sparse components using ℓ_p-minimization with $p < 1$ and reconstruct the non-sparse component using ℓ_p-minimization with $p = 2$ or $p \simeq 2$; and, finally, (5) reconstruct the desired cross-sectional image by applying the corresponding reconstruction filter bank to the partial image components obtained in the optimization process.

A function in Matlab allows the user to select the number of projections, the angle interval between two consecutive projections (angle sampling interval of incident plane waves) and the interval between two consecutive points on each projection (projection sampling interval). The example provided in Figure 1 corresponds to 24 projections taken at an interval of 180 degrees. Note that: (1) the complex conjugate of each projection is used to complete the total number of projections shown in Figure 1 (to force a real-valued solution in the space domain); and (2) the projections extend beyond the region of interest delimited by the inner square region and, for illustration purposes only, the projection sampling interval, represented in Figure 1, is small (oversampling).

A second Matlab function allows the user to specify the projection sampling interval. The sampling points inside the square region of interest shown in Figure 2 were generated at a constant interval over the projection trajectories indicated previously in Figure 1. Note that: (1) the final sampling interval in the Fourier plane follows a non-uniform sampling grid with a dense sampling interval towards the center of the figure, in contrast to a sparse sampling interval towards the borders of the square region; and (2) the horizontal scales were used to indicate the size of the Cartesian sampling grid of the cross-section being reconstructed (64×64 in the example of Figures 2).

The dense concentration of points towards the center of the Fourier plane and on the intersections of any two projections (arc trajectories) generates an ill-conditioned matrix

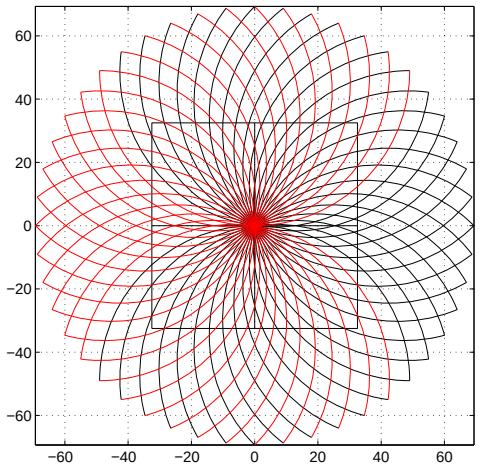

Figure 1. Projections on a square cross-section region in the Fourier plane

$\mathbf{A}\,\mathbf{A}^H$, where $\mathbf{A}$ represents the sampling matrix, that increases the reconstruction times (these points are equivalent to repeated measurements on the Fourier plane) [MvBAea09].

The user can reduce the redundancy of the sampling matrix by then applying a third Matlab function that subsamples the dense irregular grid of sampling points (Figure 2). The sampling points indicated in the square area of Figure 3 were obtained after selecting only the points in Figure 2 that are at a certain minimum distance from each other. This operation removes redundancies of the sampling points. Note that: (1) the dense arcs of circles presented in Figure 2 were reduced to fewer points in Figure 3 and all the sampling points on the intersections of any two arcs were reduced to a single point; in addition, (2) this subsampling operation preserves the complex-conjugate symmetry of the sampling points (if s is a sampling point, then its complex-conjugate value, s^*, is also a sampling point) which forces a real-valued solution of the ℓ_p-minimization (real-valued reconstructed image).

We can use the 64×64 Shepp-Logan phantom shown in Figure 4 to test our image reconstruction algorithm based on filter bank decomposition and ell_p-minimization. A fourth Matlab function computes the fractional Fourier transform of the Shepp-Logan on an irregular grid (any irregular grid) of sampling points such as in the example shown in Figure 3. These fractional Fourier coefficients are then used to simulate the measurements that we expect to obtain using our Microwave Tomographic Scanner (sampled projections in the Fourier domain). These simulated measurements on an irregular Fourier grid feed the input of a two-dimensional analysis four-channel filter bank. Figure 5 shows the block diagram of the analysis and synthesis filter banks combined to the ℓ_p-minimization operations in each subband to reconstruct the cross-sectional image of the target object. The blocks $\mathbf{H}_0$, $\mathbf{H}_d$, $\mathbf{H}_h$ and $\mathbf{H}_v$ in the analysis filter bank represent the Fourier transform of a Haar filter bank with space-domain coefficients given, respectively, by

$$\mathbf{h}_0 = \begin{bmatrix} 1 & 1 \\ 1 & 1 \end{bmatrix}, \quad \mathbf{h}_d = \begin{bmatrix} 1 & -1 \\ -1 & 1 \end{bmatrix}, \quad \mathbf{h}_h = \begin{bmatrix} 1 & 1 \\ -1 & -1 \end{bmatrix}, \quad \text{and} \quad \mathbf{h}_v = \begin{bmatrix} 1 & -1 \\ 1 & -1 \end{bmatrix}, \tag{1}$$

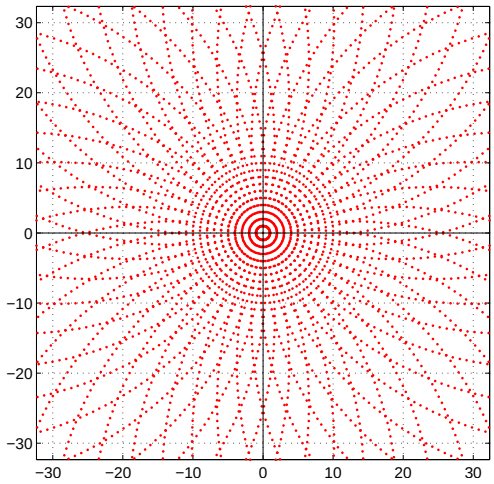

Figure 2. Dense sampling grid of the projections represented on the Fourier plane.

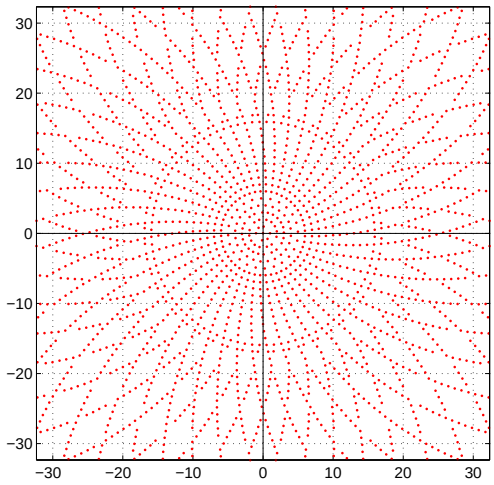

Figure 3. Dense sampling grid of the projections represented on the Fourier plane.

where h_0 corresponds to a 2D low pass-filter, h_d corresponds to a 2D filter in the diagonal direction, h_h in the horizontal direction and h_v in the vertical direction.

The outputs $\mathbf{C}_d$, $\mathbf{C}_h$ and $\mathbf{C}_v$ correspond to the sparse components of the measurements on the irregular grid of sampling points. The component $\mathbf{C}_d$ is the diagonal sparse component, $\mathbf{C}_h$ is the horizontal sparse component and $\mathbf{C}_v$ is the vertical sparse component. The component $\mathbf{C}_0$ corresponds to the non-sparse component (DC component) of the measurements on the irregular grid of sampling points. To provide an example of these components represented on a Cartesian sampling grid in the space-domain, we show in Figures 6(a) to 6(d) the analysis filter bank components $\mathbf{c}_0(m,n)$, $\mathbf{c}_d(m,n)$, $\mathbf{c}_h(m,n)$ and $\mathbf{c}_v(m,n)$ obtained by applying $\mathbf{H}_0(u,v)$, $\mathbf{H}_d(u,v)$, $\mathbf{H}_v(u,v)$, $\mathbf{H}_v(u,v)$ to the Fourier transform of the image shown in Figure 4. The frequency components $\mathbf{C}_0$, $\mathbf{C}_d$, $\mathbf{C}_h$ and $\mathbf{C}_v$ on the irregular grid of sampling points are used to reconstruct the frequency components on a Cartesian grid, $\mathbf{C}_0(u,v)$, $\mathbf{C}_d(u,v)$,

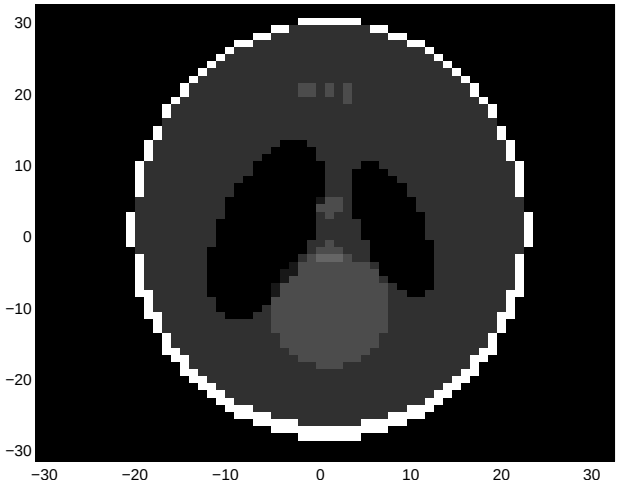

Figure 4. Shepp-Logan phantom used in the simulations: 64×64 image used to test our compressive sensing reconstruction algorithms.

$\mathbf{C}_h(u,v)$ and $\mathbf{C}_v(u,v)$, respectively. An ℓ_2-minimization function (ℓ_p-minimization function with $p=2$) reconstructs the space-domain non-sparse low-pass component $\mathbf{c}_0(m,n)$ and an ℓ_p-minimization functions, with $p<1$, reconstructs the space-domain sparse high-pass components $\mathbf{c}_d(m,n)$, $\mathbf{c}_h(m,n)$ and $\mathbf{c}_v(m,n)$. The ℓ_p-minimization problem can be represented in the general form

$$\min ||\mathbf{c}_i(u,v)||_p \text{ such that } \mathbf{A}\,\mathbf{c}_i(u,v) = \mathbf{C}_i, \tag{2}$$

where i denotes one of the components of the analysis filter bank (0, d, h and v), $\mathbf{A}$ is the fractional Fourier transformation matrix, $\mathbf{c}_i$ is the ith space-domain component on a Cartesian grid and $\mathbf{C}_i$ represents the ith frequency component of the measurements taken on an irregular sampling grid.

We used the Matlab functions developed in [MvBAea09] to solve the ℓ_p-minimization problem in (2), with $p \leq 2$. Actually, in the reconstructed components shown in Figure 7, the low-pass component $\tilde{\mathbf{c}}_0(m,n)$ was obtained with $p=1.5$ and the high-pass components with $p=0.1$. We didn't conduct a too extensive investigation on the values of p to try to improve even more our results (the remaining parameters in the Matlab function used to solve the ℓ_p-minimization problems had the standard values indicated in [MvBAea09]), but we observed that there was some flexibility in the numerical values of p. Note that: (1) the ℓ_2-minimization to find the low-pass component had, actually, $p=1.5$ ($p<2$); and the ℓ_p-minimization to find the high-pass components had $p=0.1$ (we also used $p=0.01$, with equivalent results).

Finally, a two-dimensional synthesis filter bank reconstructs the cross-sectional image of the object from the frequency components obtained in the minimization step. The analysis and synthesis filter banks used in our scheme represented in Figure 5 form a perfect reconstruction filter bank. The two-dimensional frequency response of a synthesis filter is obtained

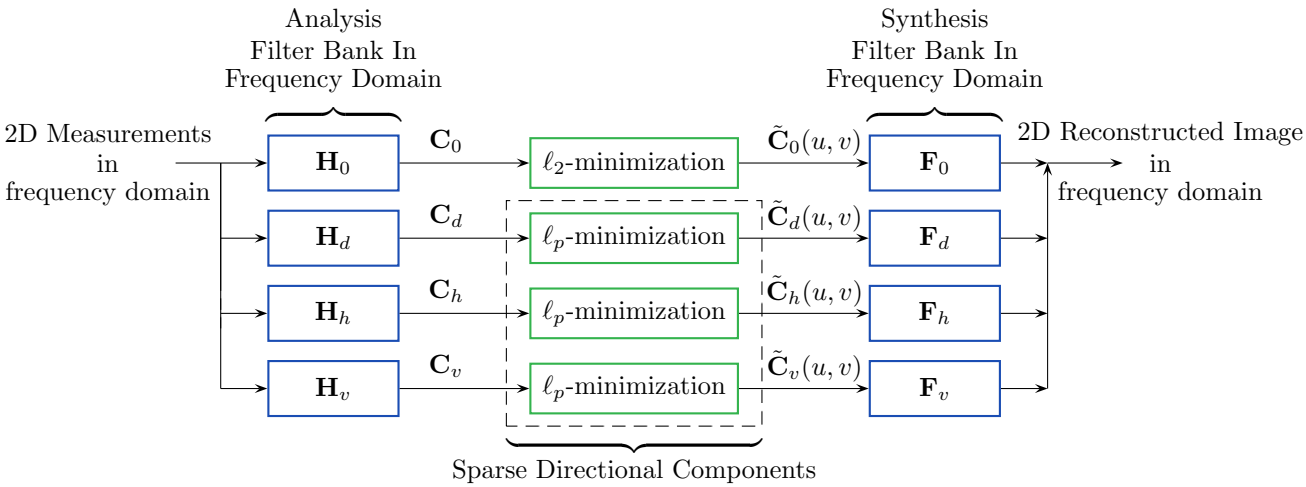

Figure 5. Analysis four-channel filter banks used to subdivide the measurements into low-pass component and directional sparse components (sparsity in the space domain) and corresponding synthesis four-channel filter bank used to reconstruct the Fourier transform of the cross-sectional image.

by taking the complex conjugate of the frequency response of the corresponding analysis filter. That is, $\mathbf{F}_i = \mathbf{H}_i^*$, for $i = 0, d, h, v$. Note that: (1) the filter banks used in our scheme are oversampled (we don't use downsampling in the analysis filter bank nor upsampling in the synthesis filter bank); (2) we tested our scheme using one set of two-dimensional Haar filter banks, but other wavelet filter banks could also be tested (see additional example in Section 1.1.1. Figure 8 shows the final reconstructed cross-sectional image represented in the space-domain.

The final reconstructed image in Figure 8 and the original Shepp-Logan phantom image in Figure 4 show small perceptual differences, but the signal-to-error rate is not high (SER = 0.1 dB). The error of the reconstructed image is higher than the reconstruction errors reported in [MvBP13] and [MvBP09]; however, the result in Figure 8 was obtained under more restrictive conditions. To limit the computation time needed for image reconstruction, we have to limit the size of the images and the number of measurements used in the reconstruction. We have to use smaller size images and fewer measurements than in previous works because now we are computing the two-dimensional Fourier transform over a non-Cartesian grid (diffraction tomographic data taken on a non-Cartesian grid) with a non-fast Fourier transform algorithm. Previous work on tomographic image reconstruction using compressive sensing assumed x-ray tomography: data collected on a rectangular grid and computations using the fast Fourier transform. The poor distribution of the measurements on a non-Cartesian grid (regions of low density sampling and regions of high density sampling) and the reduced size of the images, reducing the proportional sparsity of the images, may contribute to increase the reconstruction error; however, this problem needs further investigation.

We are investigating the following points to improve our microwave tomographic imaging

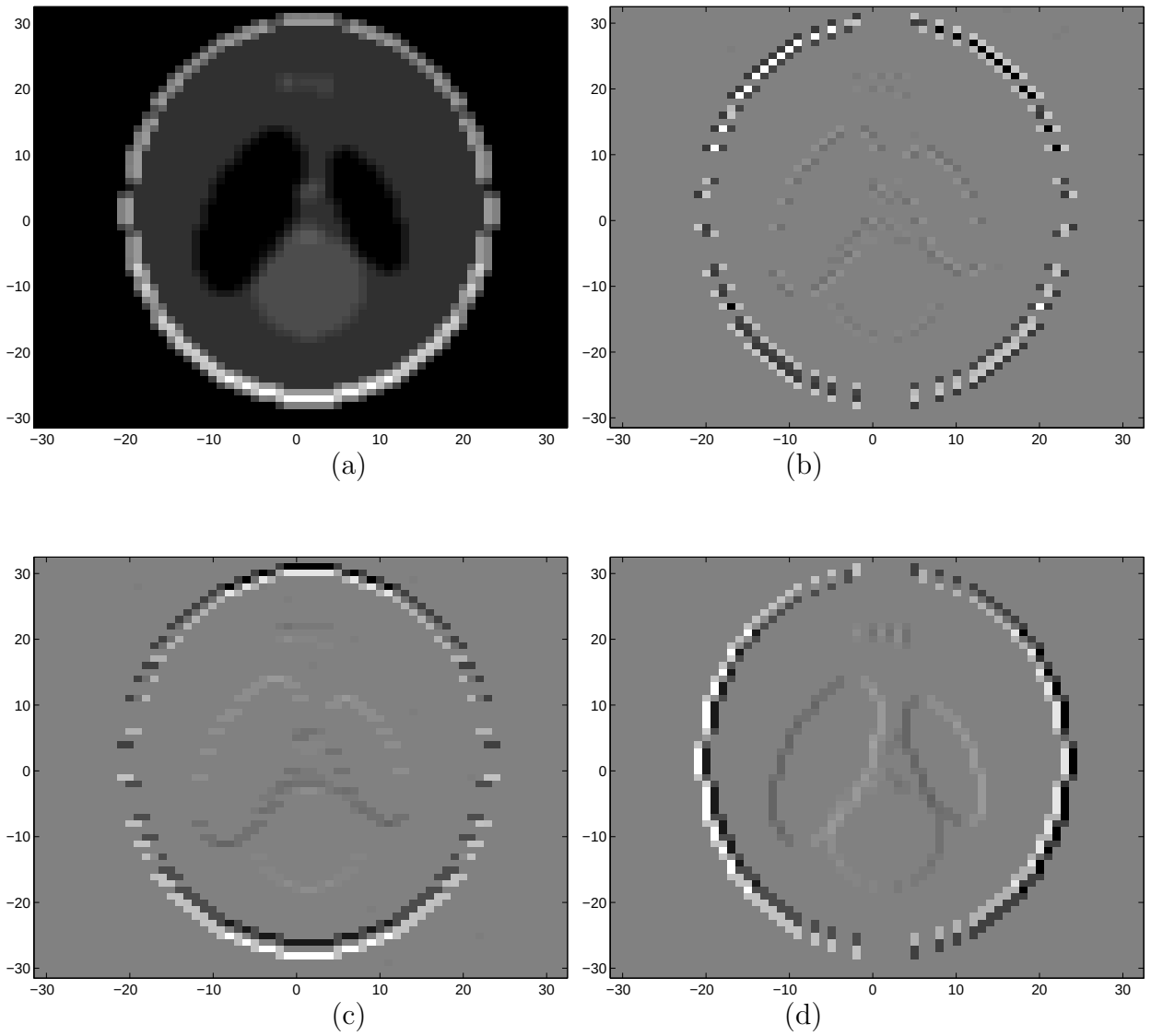

Figure 6. Components of the image shown in Figure 4 represented on a Cartesian sampling grid in the space-domain: (a) low-pass component $\mathbf{c}_0(m,n)$; (b) high-pass diagonal component $\mathbf{c}_d(m,n)$; (c) high-pass horizontal component $\mathbf{c}_h(m,n)$; and (d) high-pass vertical component $\mathbf{c}_v(m,n)$.

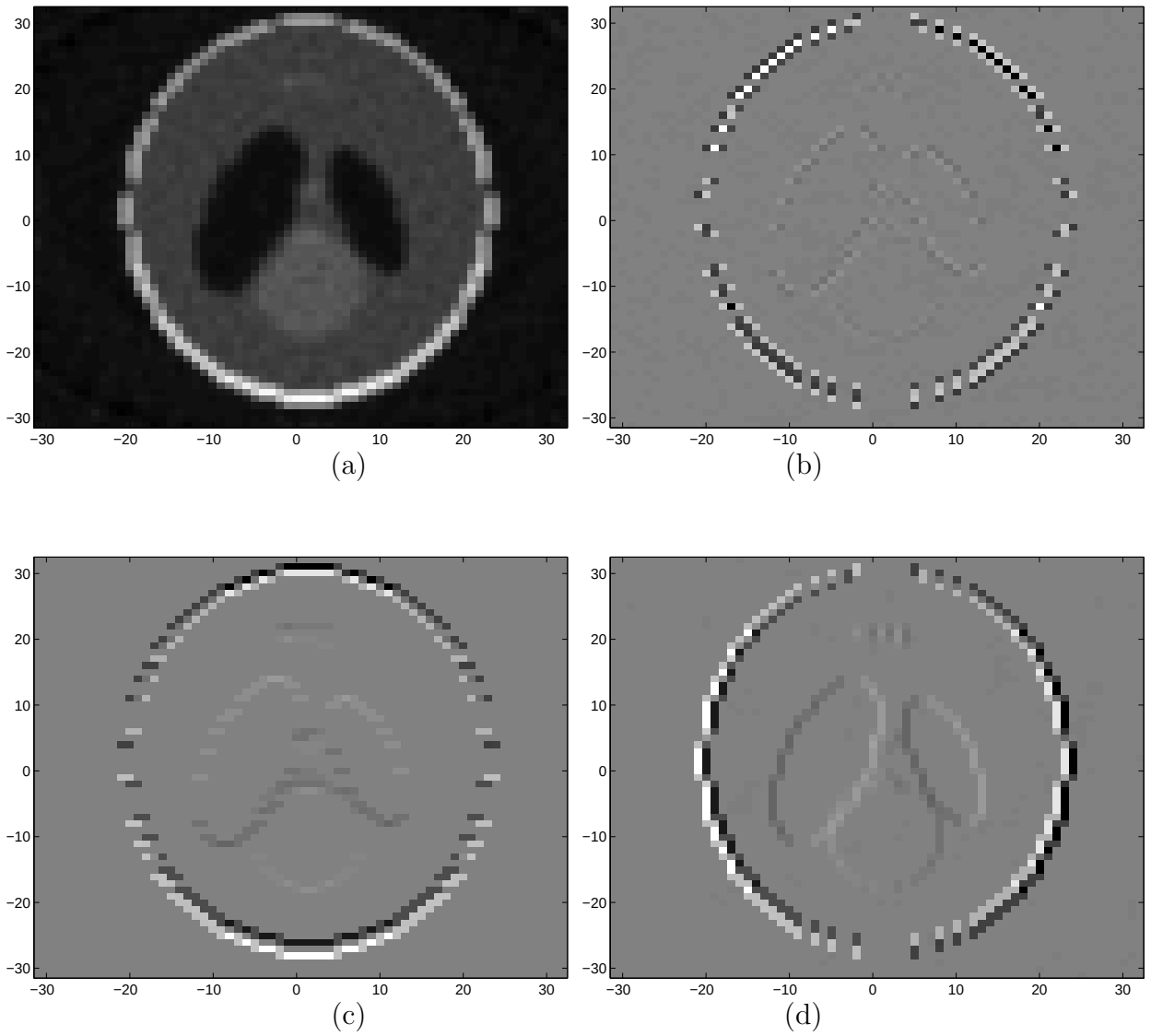

Figure 7. The components reconstructed by solving the ℓ_p-minimization problem in (2) and represented on a Cartesian sampling grid in the space-domain: (a) low-pass component $\tilde{\mathbf{c}}_0(m,n)$; (b) high-pass diagonal component $\tilde{\mathbf{c}}_d(m,n)$; (c) high-pass horizontal component $\tilde{\mathbf{c}}_h(m,n)$; and (d) high-pass vertical component $\tilde{\mathbf{c}}_v(m,n)$.

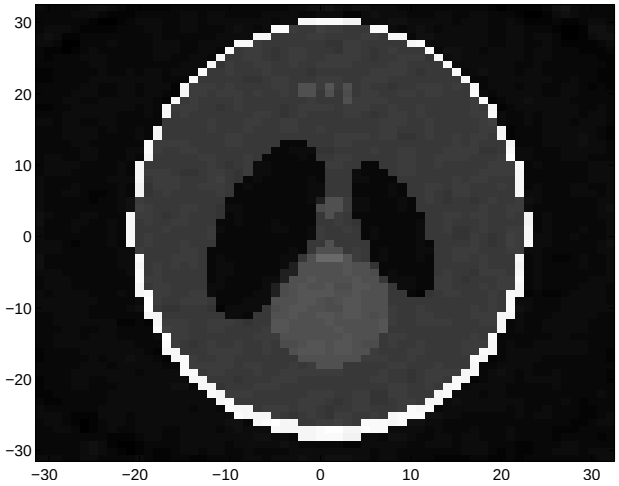

Figure 8. The reconstructed Shepp-Logan phantom.

scheme:

- faster computation of the fractional Fourier transform;
- other families of FIR filter banks to generate sparse components;
- optimization of the irregular grid of sampling points in the Fourier plane (we already implemented this optimization in Matlab); and
- image reconstruction using real-world measurements (collected with our microwave tomographic scanner).

1.1.1 Compressive Sensing with Prior Information

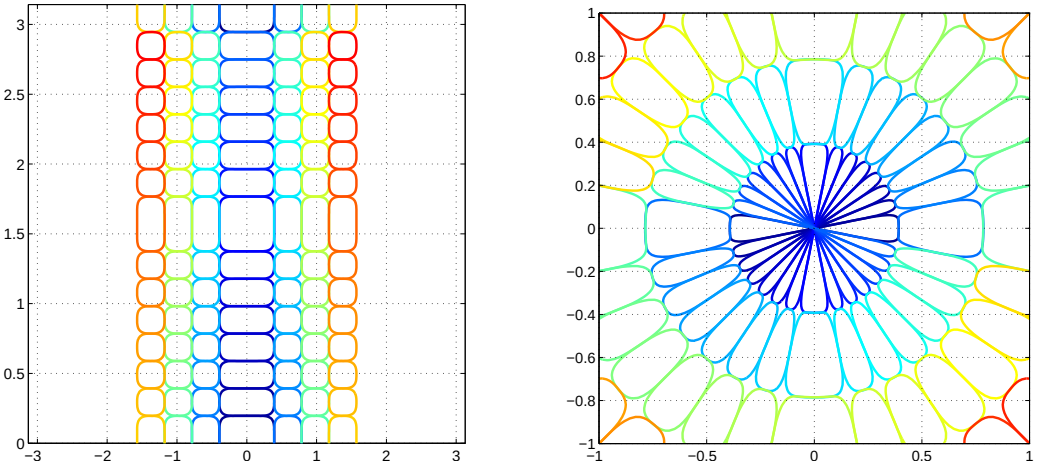

Figure 9. Tiling of the Fourier plane by using the radon transform and cosine modulated filter bank: (a) representation of bandpass frequency responses in the radon domain (sinogram); and (b) corresponding directional decomposition in the Fourier plane [vBMP07].

We used directional decomposition of the measurements taken in the Fourier plane to implement a scheme for tomographic image reconstruction using compressive sensing with

prior information. The use of compressive sensing with prior information, as proposed in our research objectives, targeted two points: (1) faster data collection – reduction of the number of measurements required to reconstruct the original tomographic image; and (2) faster image reconstruction.

We add prior information by implementing an iterative reconstruction of the original tomographic image. The partial image reconstructed obtained from some of the directional components of the original image (obtained with the measurements filtered in a certain direction) are used as prior information for the reconstruction of new directional component of the image. The tiling of the Fourier plane indicated in Figure 9 was used to implement the directional image decomposition ant the iterative image reconstruction using compressive sensing with prior information.

Note that to solve the ℓ_p-minimization problem in (2) we have to compute a fractional Fourier transform represented by the matrix $\mathbf{A}$. The size of this matrix depends on the number of measurements taken in the Fourier plane over the arc trajectories of the projections. By carefully reducing the number of measurements and in this way the size of the matrix $\mathbf{A}$, we can both simplify the acquisition processes and reduce the time required to solve the ℓ_p-minimization problem with prior information for each one of the directional components of the tomographic image.

However, this scheme for compressive sensing with prior information did not not generate the expected benefits. We could not observe any meaningful improvement neither in the reduction of the number of measurements needed for image reconstruction nor in the reduction of computation times. Two points could be raised to explain the observed deficiency of our scheme. The first point is related to the filter bank and directional filtering and the second to prior information selection.

The sharp transition region of the frequency responses generated by the cosine modulated filter bank used in the directional filtering, indicated in Figure 9, actually, contribute to destroy the sparsity in the space domain making the reconstruction with prior information less effective. To address this issue in our research, we also extracted prior information with the filter bank in (1) that has very short length filters. In this case, the loss of directionality in the filter bank decomposition, compared to the filter bank used to generate the plots shown if Figure 9, contributed again to not any noticeable benefit in the use of compressive sensing with prior information. The other point to explain the deficiency of our proposed scheme concerns prior information selection. The selection of points in the space domain from a partial reconstruction of the original image, based on their magnitude value above a certain threshold, is clearly not working as effective prior information for the compressive sensing algorithm and this selection needs further refinement.

The use of compressive sensing with prior information in the context of underground penetrating radar and microwave tomography requires further investigation into the proposed scheme based on directional image decomposition.

1.1.2 Journal Paper

C. Jacques Miosso, R. F. von Borries, and J. H. Pierluissi. Compressive Sensing with Prior Information − Requirements and Probabilities of Reconstruction in ℓ_1-Minimization." *IEEE Transactions on Signal Processing*, pages 2150–2164, May 2013.

- Abstract − In compressive sensing, prior information about the sparse representation's support reduces the theoretical minimum number of measurements that allows perfect reconstruction. This theoretical lower bound corresponds to the ideal reconstruction procedure based on ℓ_0-minimization, which is not practical for most real-life signals. In this paper, we show that this type of prior information also improves the probability of reconstruction from limited linear measurements when using the more practical ℓ_1-minimization procedure, for the same considered stochastic signal. In order to prove this result, we present the necessary and sufficient conditions for signal reconstruction by ℓ_1-minimization when using prior information, for the particular case in which the measurement domain and the sparse representation domain are related by the discrete Fourier transform (DFT). We then prove that the lower bound for the probability of attaining these conditions increases with the number of support locations in the prior information set, and obtain the expression for the final probability of reconstruction under specific conditions. The numerical simulations also include the case of a general orthogonal transform, with equivalent results.

1.1.3 Conference Paper

The collaborators Berenice Verdin and von Borries created successfully an approach for sensing with compression (compressive sensing) and prior information in full waveform lidar that is able to reconstruct the complete range profile of lidar returns. In that research, Verdin was supported by the National Geospatial-Intelligence Agency (NGIA). Two related papers are listed below.

B. Verdin and R. von Borries. Lidar compressive sensing using chaotic waveform. In SPIE 9077, Radar Sensor Technology XVIII, Baltimore, MD, May 5–9 2014. [VvB14].

- Abstract − Full waveform Lidar systems have the ability of recording the complete signal reflected from the illuminated target. Therefore, more detail information can be obtained compared to conventional Lidar systems. The problem that is faced in using full waveform Lidar is the acquisition of high volume data, a solution proposed to solve this problem is compressive sensing. By using a compressive sensing approach we can reduce the sampling rate and still be able to recover the signal. The reduction is incorporated in the acquisition hardware, where we perform sensing of the signal with compression. In this paper we propose to use a deterministic compressive sensing approach by using a chaotic signal as the sensing matrix. The proposed approach gives the range profile information without the requirement of further processing techniques.

For comparison we used two different types of transmitted signals: chaotic and Linear Frequency Modulated (LFM) signals. Simulations demonstrate that chaotic signals give better results than the LFM signals. By using a chaotic signal we can obtain the impulse response of the target by using less than 20 percent of the samples.

B. Verdin and R. von Borries. Lidar range profile reconstruction by using chaotic signals and compressive sensing. In SPIE 8512, Infrared Sensors, Devices, and Applications II, San Diego, CA, August 12 2012. [VvB12].

- Abstract − Full waveform lidar systems are capable of recording the complete return signal from the laser illuminated target. By making use of the return full waveform, one can obtain more detailed information about the target of interest than the simple target range. The development of better methods to extract information from the return signal can lead to better target characterization. Several methods have been proposed in the literature to obtain the complete range profile or radar cross section of the target.1, 2 In a previous work, we proposed to use a compressive sensing scheme to acquire and compress the received signal, and at a post-processing stage reconstruct the signal to obtain the range profile of the target. We extend this previous work on full waveform lidar using chaotic signal by including additive white Gaussian noise into the acquisition stage of the lidar system. The objective is to test the robustness of the previously developed approach based on compressive sensing to different noise level intensities. The simulation software Digital Imaging and Remote Sensing Image Generation (DIRSIG) was used to simulate the range profile corresponding to a three-dimensional scene. The simulation results indicate that the full range profile can be reconstructed with a compressive sensing acquisition as low as 25 percent of the total number of samples and with low root-mean-square error (RMSE). The proposed lidar system with compressive sensing can be used to sense with compression and recover the range target profile.

1.1.4 Summary

We were able to complete the image reconstruction using measurements over a non Cartesian grid and fractional Fourier transform (journal paper and PhD dissertation under preparation). However, the scheme with prior information to reduce the number of measurements and the computation time was not successful and it needs further investigation.

1.2 Objective 2

To determine if compressive sensing can reconstruct parts of the image that are missed with standard algorithms.

Figure 10(a) shows a sparse image used in our preliminary Matlab simulations of tomographic image reconstruction. The reconstructed image using filtered back projection

algorithm with measurements taken over straight line projections (as in x-ray tomography) at 24 angles is very poor, as illustrated in the example of Figure 10(b). Our results of image reconstruction using compressive sensing and measurements taken over circular trajectories obtained from simulation of the direct microwave diffraction problem shows compelling improvements. The reconstructed image in the example of Figure 10(c) was obtained using compressive sensing with measurements taken over circular trajectories (diffraction tomography) at 24 equally spaced angles. Comparing Figures 10(c) and (b), we can notice clear improvements obtained with compressive sensing when compared to a basic tomographic image reconstruction technique.

1.2.1 Summary

Our tomographic image reconstruction algorithm based on compressive sensing outperforms standard algorithms (higher signal-to-error ratio, SER). However, further tests with real ultra wideband radar data need to be conducted.

1.3 Objective 3

To evaluate the computational expense of image reconstruction with compressive sensing.

We used Matlab to compute the ℓ_p-minimization discussed in Section 1.1 on a single core with 2667 MHz and 2 GB of a computer node of the Distributed Computing Lab (DCL). We are working with the DCL to reduce the total time required to complete the reconstruction based on compressive sensing; however, the implementation using DCL depends on the final algorithm for compressive sensing with prior information.

1.3.1 Summary

Our algorithm is computationally intensive even using prior information and distributed computing. Image reconstruction in real-time is not feasible with the current algorithm.

1.4 Objective 4

To integrate compressive sensing into a practical ground penetrating radar with ultra-wideband technology.

The team formed by M. Rojas, R. Barreto, C. Soto, G. Gonzalez, V. Jimenez, J. Pierluissi and R. von Borries worked on the development of the microwave tomographic scanner design. Our microwave tomographic scanner is going to use a commercial stepper motor positioning control (including stepper motors, controller and drivers and programming software interface). The final block diagram is represented in Figure 11. Figure 12 shows the three-dimensional view (sketched in Google SketchUp software) of the mechanical positioning system used in the microwave tomographic scanner and represented in simplified form by the block "Sand Box" in Figure 11. The positioning control of the tomographic polar

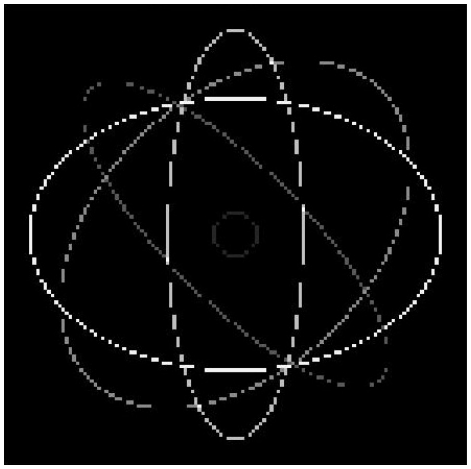

(a)

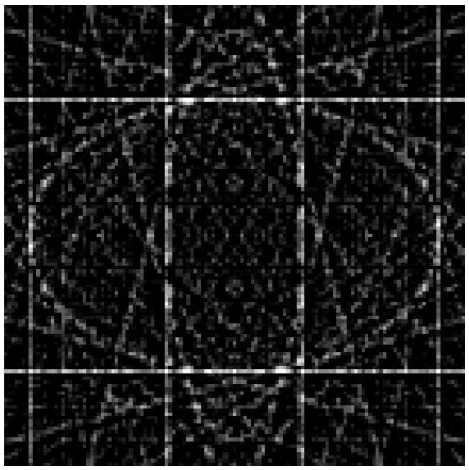

(b)

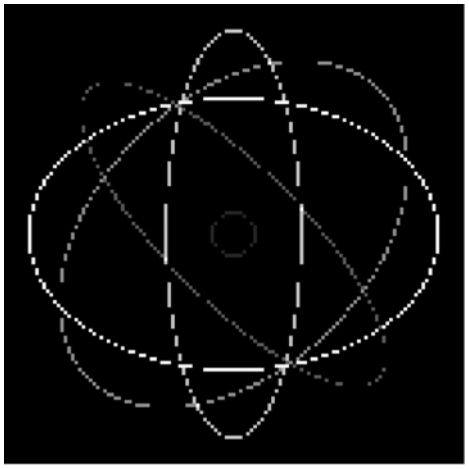

(c)

Figure 10. Image reconstruction with traditional filtered backprojection algorithm and compressive sensing: (a) original sparse image; (b)reconstruction using filtered backprojetion algorithm and 24 straight line projections; and (c) reconstruction using compressive sensing and 24 circular projections. The same number of measurements was used in (b) and (c).

coordinate (ρ, θ) of the sand box represented in Figure 12 uses a complete commercial solution. Note that most of the small parts of this system, including the commercial stepper motor positioning control, were acquired with funding available to the MSPL, Multi Sensing Processing and Learning Lab, directed by PI von Borries.

1.4.1 Acquisition System Final Specification

- **Waveform generator**

  1. AWG7122C – arbitrary waveform generator, 12 GSamples/s, 10 bits resolution and two channels
  2. AWG7122C06 – interleaved high bandwidth output
  3. AWG7122C08 – fast sequence switching

  The AWG7122C generates complex wideband signals across a frequency range of up to 9.6 GHz with the two options (1) interleaved high bandwidth output AWG7122C06 and (2) fast sequence switching AWG7122C08 (up to 24 GSamples/s with these two options). In addition, it has vertical resolution up to 10 bits. The user interface based on Windows 7, enables the easy creation of arbitrary waveforms including Gaussian pulses, first and second derivatives of Gaussian pulses (commonly used in ground penetrating radar), and modulated versions of these waveforms. In this way, the complex waveforms can be adjusted to compensate the intrinsic characteristics of our system and the propagation media (pre-distortion of the arbitrary waveforms generated). In addition, this arbitrary waveform generator enables creation of infinite waveform loops and enhances the ability to replicate real-world signals. This instrumentation supports network integration and USB ports for easy integration with a personal computer (PC).

- **Waveform digitizer**

  1. DSA8300 – digital serial analyzer.
  2. 80E07 – two remote sampling modules; two channels each, 30 GHz.

  The DSA8300 digital sampling oscilloscope has A/D conversion with the best vertical resolution, 16 bits, and very low time-base jitter of 425 fs on the 4 simultaneously acquired channels with the two remote sampling 80E07 (and the total number of channels can be expanded to up to 8, if two more remote sampling modules are added to the current configuration). The DSA8300 has three acquisition modes: sample, envelope and average. The average mode can be useful working with low amplitude signals returned from our application in ground penetrating radar. The two 80E07 are 30 GHz sampling modules, with low-noise signal acquisition (300 μV at 30 GHz), fast rise time (11.7 ps from 10% to 90%), and dynamic range of 1 V_{pp}. Finally, the input impedance of each channel is 50 Ω.

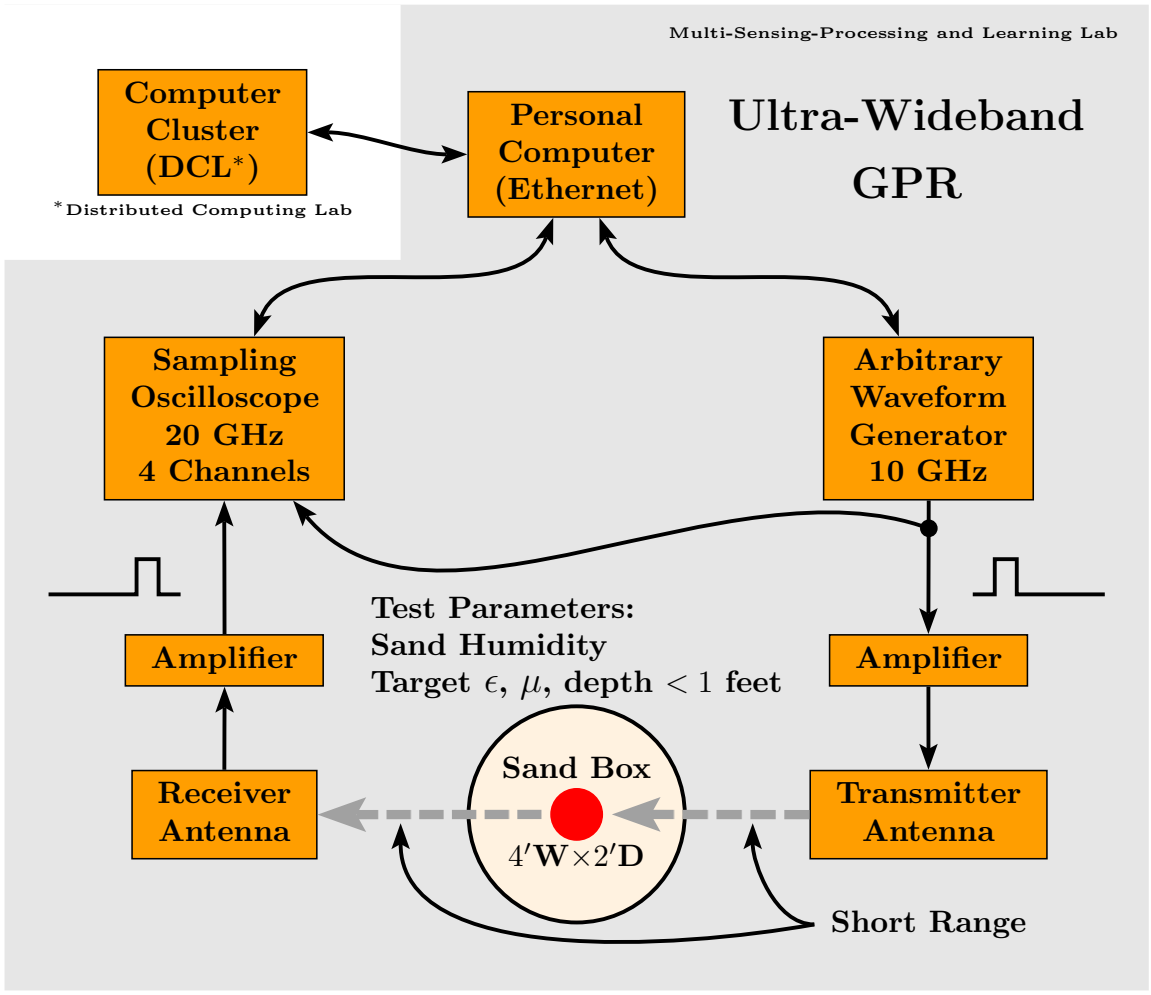

Figure 11. Ground penetrating radar system.

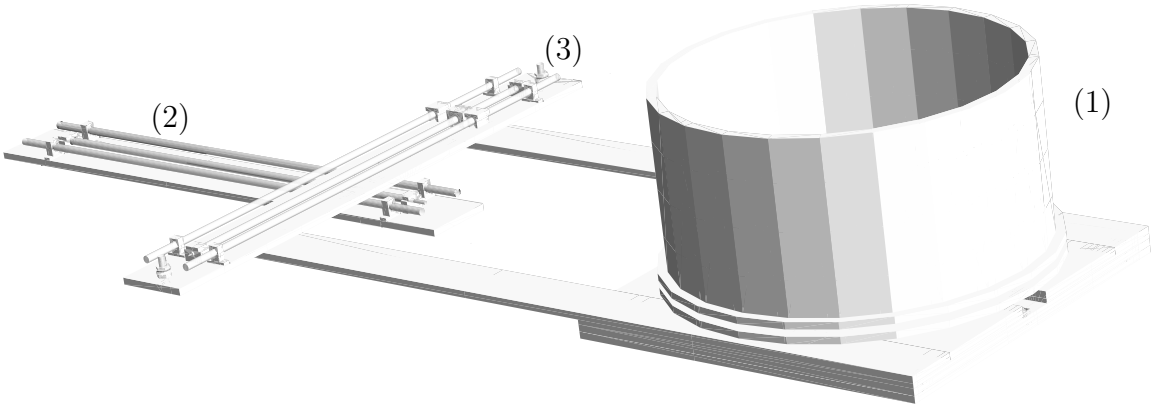

Figure 12. Microwave tomographic scanner showing: (1) sand box; (2) linear positioning stage (ρ component of the tomographic projection); and (3) angular positioning stage (θ component of the tomographic projection). Stepper motors and antennas are not represented.

- **Antennas** We conducted research on the types of antennas to use in our system for ground penetrating radar, and, initially, we had considered two types of antennas: Vivaldi and horn. In our laboratory tests, we concluded that the Vivaldi antenna is not a viable alternative, basically due to its poor directivity. We decided to use horn antennas, however, they are more expensive and difficult to design than the Vivaldi. Currently, we still don't have the resources to purchase these antennas.

    1. Horn antenna – Horn antennas have also wide frequency response and good directivity (better than Vivaldi antennas), however, they are more expensive and difficult to manufacture. We are considering to buy a couple of used horn antennas. Horn used antennas can be found a relatively low price providing good frequency response.

- **Amplifiers**

    1. 5866-107 (Picosecond) – linear amplifier with gain 26 dB and bandwidth from 2.5 kHz to 10 GHz; high gain with low power dissipation (1.7 W at +17 dBm); linear output greater than 4 V_{pp}; RF input SMA jack and RF output SMA jack, 50 Ω matched.
    2. BZP112UB1 (B&K Technologies) – linear amplifier with gain 26 dB and bandwidth from 0.1 MHz to 12 GHz; low noise figure 1.7 dB maximum and gain flatness of ±1.2 dB maximum; output power 10 dBm; group delay ±15 ps in the range 2 GHz to 12GHz; RF input SMA jack and RF output SMA jack, 50 Ω matched.

    These two amplifiers were purchased with funds provided by the Office of Sponsored Projects (ORSP) of the University of Texas at El Paso (UTEP).

- **RF cables**

    1. Semi-flexible coaxial cable (Picosecond) – electrical performance comparable to semi-rigid; SMA 50 Ω; maximum frequency 26 GHz and low power attenuation 40 dB per 100 ft at 8 GHz; bends easily by hand; 100% shielded by two metal jackets for low leakage. Only one cable 18 inches long was purchased at this point with funds provided by the Office of Research and Sponsored Projects (ORSP) of the University of Texas at El Paso (UTEP). The remaining cables will be acquired with funds of project W911NF-11-1-0129, after the whole system is assembled and we obtain a more precise estimate of the lengths for all the cables required.

- **Sand box**

    We built a sand box out of a large plastic container and it is going to be installed in the MSPL Lab to test our experimental setup.

The team formed by M. Rojas, R. Barreto, C. Soto (investigators working in the first phase of the microwave scanner project), V. Jimenez, G. Gonzalez and A. Orea (working in the second phase of the microwave scanner project) and R. von Borries and Pierluissi worked on the development of the microwave tomographic scanner. We completed the design and are in the process of assembling the microwave scanner.

1.4.2 Low-Cost GPR System

Three undergraduate students developed a low-cost GPR system based on the USRP N210 hardware (by Ettus Research), Vivaldi antennas (built in our lab) and software programming language Labview (by National Instruments). The students were partially supported by the University of Texas System Louis Stokes Alliance for Minority Participation (LSAMP), funded by the National Science Foundation (NSF), and by the National Center for Border Security and Immigration (NCBSI), funded by the Department of Homeland Security (DHS). The project is part of an ongoing effort to promote **research** and **education** on radar systems, and it will be used in our project in the preliminary tests of antennas and during preliminary tests of ground penetrating radar data acquisition, before using the more expensive instrumentation. Figure 13 shows the low-cost GPR system connected to a desktop computer.

1.4.3 Conference Paper

"Platform for Research and Education on Ground Penetrating Radar," M. J. Salvador, V. Jimenez, R. G. Lopez, R. von Borries, Proceedings of the SPIE, Volume 8714, id. 87141K, 9 pp. (2013) [SJLvB13].

- Abstract − Current commercial Ground Penetrating Radar (GPR) systems are found at a high cost and allow little interaction between the user and the system. This paper presents a low cost and flexible GPR platform attractive for use in education and research based on the Universal Software Radio Peripheral (USRP) developed by Ettus Research. A software application developed in Labview enables users to select and modify fundamental parameters of the transmission and reception stages of a GPR system. Users are able to modify parameters such as sampling and carrier frequencies, waveform shape, amplitude, and bandwidth. The programmability of the USRP in conjunction with the developed software tools provides a user-friendly GPR platform.

1.4.4 Summary

The construction of our ground penetrating radar incorporating tomographic acquisition proved to be quite challenging. We needed to make several changes to complementary components needed for the scanner due to: (a) non-availability; or (2) high costs. We made good progress in the tomographic scanner but it is still under construction.

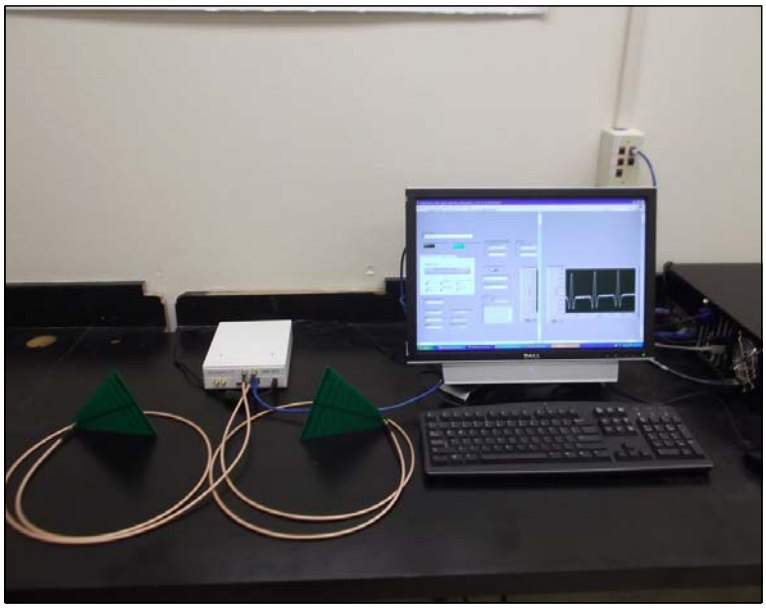

Figure 13. Low-cost GPR system.

2 Teaching Excellence and Innovation in Support of the Research

A valuable component of our project was to improve and speed up learning by UTEP's students in areas needed for this project. Addressing this objective, Dr. von Borries in collaboration with Dr. Patricia A. Nava (Associate Dean for Academic Affairs & Undergraduate Studies in the College of Engineering and also member of our ECE department) and Dr. Berenice Verdin, Postdoctoral Fellow for Teaching Excellence and Innovation, worked on integrating new teaching technologies in the following course undergraduate course:

- Continuous-Time Signals and Systems – Summer of 2012, Fall 2012, Spring 2013, Fall 2013 and Spring 2014.

Note that our new learning environment can be extended to other classes in Electrical Engineering at either undergraduate or graduate levels such as cross-listed as graduate and undergraduate course:

- Advanced Radar – it included material on ground penetrating radar and was taught twice, in the Spring 2013 and the Spring 2014.

The new teaching environment included four technologies:

- Connexions – composing a textbook for continuous-time signals and systems.
- Interactive Lablets – interactive Mathematica simulation modules in CDF–Computational Document File.

- Quadbase – questions and answers in continuous-time signals and systems.
- OpenStax Tutor – assessing students learning.

The use of these technologies provided the following main benefits: (1) increased effective learning; (2) easy customization of low-cost high-quality material to meet individual students' needs; and (3) assessment tools that enabled the instructor to focus teaching efforts on areas that students need most [MBVvB14].

2.1 Conference Abstract

"Improving Engineering Education at UTEP: Initial Implementation," B. Verdin, R. von Borries and P. Nava, The International Sun Conference on Teaching and Learning, February 28 to March 1, 2013, El Paso Texas. The undergraduate student E. Estrada worked as a teaching assistant with von Borries.

- Abstract – UTEP has teamed with the "Signal Processing Education Network," (SPEN), in the implementation, assessment and evaluation of the use OpenStax Tutor. This platform incorporates three technologies: Connexions, Interactive Lablets, and Question/Response System to improve teaching and learning. OpenStax Tutor seeks to develop materials that allow educators to break away from traditional textbook-lecture-and-homework-based education, and create a new framework based on an engaged community of educators, students, and industry professionals that continuously collaborate, improve, and explore interactive content. During the fall semester of 2012, the team of faculty at UTEP implemented a sophomore course on continuous-time signals and systems using the OpenStax Tutor.

2.2 Supporting Proposal

Note that Dr. Verdin was supported by UTEP, or more specifically:

- Postdoctoral Fellowship for Teaching Excellence and Innovation, P. A. Nava (PI), R. von Borries (Co-PI), University of Texas at El Paso, UTEP's Provost Office, $80,000, from June 2012 to May 2014. We started the project funded by the UTEP's Provost Office in the Summer of 2012.

References

[MBVvB14] H. G. Mullet, A. C. Butler, B. Verdin, and R. von Borries. Delaying feedback promotes transfer of knowledge despite student preferences to receive feedback immediately. *Journal of Applied Research in Memory and Cognition*, 2014.

[MvBAea09] C. Jacques Miosso, R. F. von Borries, M. Argáez, and L. Velazquez et. al. Compressive sensing reconstruction with prior information by iteratively reweighted least-squares. *IEEE Transactions on Signal Processing*, 57(6):2424–2431, June 2009.

[MvBP09] C. J. Miosso, R. F. von Borries, and J. H. Pierluissi. Compressive sensing method for improved reconstruction of gradient-sparse magnetic resonance images. In *42nd Asilomar Conference on Signals, Systems, and Computers*, Pacific Grove, CA, November 2009.

[MvBP13] C. Jacques Miosso, R. F. von Borries, and J. H. Pierluissi. Compressive sensing with prior information - Requirements and probabilities of reconstruction in ℓ_1-minimization. *IEEE Transactions on Signal Processing*, pages 2150–2164, May 2013.

[SJLvB13] M. Salvador, V. Jimenez, R. Lopez, and R. von Borries. Plataform for research and education on ground penetrating radar. In *SPIE Radar Sensor Technology XVII*, volume 8714, Baltimore, MD, May 31 2013.

[vBMP07] R. F. von Borries, C. Jacques Miosso, and C. Potes. Directional filter banks for wavelet decomposition of images based on the Radon transform. In *41th Asilomar Conference on Signals, Systems, and Computers*, pages 2095–2099, Pacific Grove, CA, November 2007. Invited paper.

[VvB12] B. Verdin and R. von Borries. Lidar range profile reconstruction by using chaotic signals and compressive sensing. In *SPIE 8512, Infrared Sensors, Devices, and Applications II*, San Diego, CA, August 12 2012.

[VvB14] B. Verdin and R. von Borries. Lidar compressive sensing using chaotic waveform. In *SPIE 9077, Radar Sensor Technology XVIII*, Baltimore, MD, May 5–9 2014.